Nanotechnology **19** (2008) 035603 (6pp) doi:10.1088/0957-4484/19/03/035603

Efficient field emission from vertically grown planar ZnO nanowalls on an ITO–glass substrate

D Pradhan[1], M Kumar[2], Y Ando[2] and K T Leung[1,3]

[1] WATLab and Department of Chemistry, University of Waterloo, Waterloo, ON, N2L 3G1, Canada
[2] Department of Materials Science and Engineering, Meijo University, Nagoya 468-8502, Japan

E-mail: tong@uwaterloo.ca

Received 4 July 2007, in final form 30 October 2007
Published 11 December 2007
Online at stacks.iop.org/Nano/19/035603

Abstract

Vertically grown planar ZnO nanowalls, with typical dimensions of 40–80 nm thickness and several micrometers wide, were electrodeposited on an indium–tin-oxide (ITO)–glass substrate at 70 °C. X-ray photoelectron spectroscopy (XPS) studies reveal that the nanowalls consist of ZnO covered with a $Zn(OH)_2$ overlayer. An x-ray diffraction (XRD) study shows that these nanowalls have the wurtzite structure and are highly crystalline. The corresponding Raman and photoluminescence spectra further indicate the presence of oxygen deficiency. These ZnO nanowalls exhibit excellent field emission performance, with not only a considerably lower turn-on field of 3.6 V μm^{-1} (at 0.1 $\mu A\ cm^{-2}$) but also a higher current density of 0.34 mA cm^{-2} at 6.6 V μm^{-1} than most ZnO nanowires and other one-dimensional nanostructures reported to date.

(Some figures in this article are in colour only in the electronic version)

1. Introduction

There has been extensive research in the last two decades on electron field emission (FE) from one-dimensional (1D) materials because of their high aspect ratios. It is well known that besides the geometric factors, thermal stability at low vacuum is equally important for the operation of field emitters. Among the 1D materials, carbon nanotubes have attracted a lot of attention due to their promising potential in display technology [1, 2]. However, some notable disadvantages with carbon nanotubes lie in their high-temperature synthesis method and the instability of nanotube tips at low vacuum. As an oxide, zinc oxide (ZnO) not only has a high melting point but also is thermally and chemically stable, making it one of the most widely used materials for varistors [3]. The ZnO nanostructures have also been reported to exhibit stronger endurance to oxygen medium than carbon nanotubes in the FE process [4]. It is therefore of great practical interest to develop novel ZnO nanostructures with high FE performance. Previous FE studies on ZnO material have focussed on ZnO nanowires and other 1D structures synthesized by chemical vapor deposition (CVD) at a temperature well above 600 °C [5–8]. Although two-dimensional ZnO nanosheets [9–11], nanoplates [12–14] nanodisks [15] and nanowalls [16] have also been grown by using CVD and other deposition techniques, no efforts were made to determine their FE properties except for the very recent work of Cao *et al* that shows limited FE from ZnO nanosheets [10]. In the present work, we report the synthesis of unique two-dimensional ZnO nanowalls, grown almost vertically on an indium–tin-oxide (ITO) coated glass substrate by using a simple technique involving electrochemical deposition at 70 °C, i.e. a temperature considerably lower than that used in the CVD method (600–1000 °C). These ZnO nanowalls are found to exhibit promising FE characteristics appropriate for application in display technology.

[3] Author to whom any correspondence should be addressed.

2. Experimental details

The electrochemical deposition experiments were carried out in a conventional three-electrode cell immersed in a water bath held at 70 °C. The working electrode was single-side polished, SiO_2-passivated float glass (10 × 10 mm^2) coated with an ITO film (200–500 nm thick with a sheet resistance R_s = 4–8 Ω). An aqueous solution of 0.1 M $Zn(NO_3)_2{\cdot}6H_2O$ mixed with 0.1 M KCl was used as the electrolyte and the deposition was carried out for 1 h. A potentio/galvanostat electrochemical workstation was used to deposit the nanostructure by amperometry potentiostatically at −1.1 V relative to the Ag/AgCl reference electrode, with a Pt wire acting as the counter electrode. After deposition, the resulting nanodeposits were thoroughly rinsed with Millipore water and dried under a nitrogen gas blow. The morphology of the ZnO nanowalls and their elemental composition were characterized with scanning electron microscopy (SEM) and energy-dispersive x-ray (EDX) analysis respectively, while their crystal structures were analyzed with glancing-incidence x-ray diffraction obtained with Cu Kα radiation (1.54 Å) at an incidence angle $\omega = 0.3°$. X-ray photoelectron spectroscopy (XPS) was used to analyze the chemical state composition of the as-grown nanowalls as a function of sputtering time. The optical properties of the nanowalls were examined by Raman spectroscopy using a 532 nm laser wavelength and by fluorescence spectroscopy with an excitation wavelength of 254 nm. The FE properties of the nanowalls were measured in a conventional parallel-plate diode configuration with the ZnO nanodeposit as the cathode and a stainless steel rod (with a flat circular base of 1.5 mm diameter) as the anode at a chamber pressure of 2.2 × 10^{-6} Torr [17]. With the cathode-to-anode distance kept at 0.5 mm, the FE current was measured by using a picoammeter as a function of negative voltage applied to the cathode.

3. Results and discussion

Figure 1 shows the SEM images of ZnO nanodeposits on the ITO–glass substrate obtained in a 0.1 M $Zn(NO_3)_2{\cdot}6H_2O$ solution mixed with 0.1 M KCl. Evidently, well-defined two-dimensional wall-like nanostructures with a wall thickness of 40–80 nm are found to grow nearly perpendicular on the substrate, with some of these nanowalls slightly tilted at an angle to the substrate. Figure 1(a) also shows groups of parallel, near-vertical planar nanowalls with lengths varying from hundreds of nanometers to several micrometers. The corresponding thickness of the nanowalls film, illustrated in cross-sectional SEM images (figure 1(b)), is measured to be ∼50 μm (over a total deposition time of 1 h). It is important to note that individual nanowalls are normally 5–10 μm in height and length and appear to be growing one on top of another (figure 1(b1)). Furthermore, no buffer layer is formed on the ITO–glass prior to the formation of the nanowalls (figure 1(b2)). The lateral growth of these nanowalls appears to cease when one nanowall meets another with a preferred angle between 60° and 90° (figure 1(c)). It should be noted that at a lower Zn electrolyte concentration of 0.05–0.06 M, two-dimensional ZnO nanoplates [13, 14] and nanosheets [10] have been recently reported, and the growth of these nanostructures appeared to be randomly oriented and to terminate without any physical obstructions. This may be due to slower growth kinetics at the lower electrolyte concentration, unlike the present work that uses a higher concentration (0.1 M). We have also carried out deposition at a lower Zn electrolyte concentration of 0.05 M, which also produced randomly oriented two-dimensional disk-like nanostructures but evidently in stacked arrangement. However, at a very high electrolyte concentration of 0.5 M, nanowalls as thick as ∼1 μm were obtained. The Zn electrolyte concentration of 0.1 M is found to be nearly optimal for producing well-defined, uniformly distributed near-vertical nanowalls with high reproducibility. In addition, some of the nanowalls in the present work appear to merge as double-walls (see arrows in figure 1(d)). The surface of the nanowall ledge is found to be generally smooth, as shown in figure 1(e). The inter-wall gaps of 200–800 nm observed in these self-assembled nanowalls are especially advantageous for FE applications because the screening effect normally observed in close-packed nanostructures can be minimized [18]. Lao *et al* has also reported the growth of vertical nanowalls in the presence of gold catalysts on a sapphire substrate at 875–950 °C using a thermal evaporation and condensation method [16]. These nanowalls appear to be curved and flake-like, and are interconnected with one other, forming a network. The present work therefore demonstrates that the present nanowalls not only can be obtained by electrodeposition at a considerably lower temperature, without the need of catalysts or lattice matching (to a compatible substrate), but also can be produced in distinct well-defined vertical planar entities. Figure 1(f) shows the corresponding EDX spectrum of these nanowalls. The O-to-Zn atomic ratio (∼1.7) is found to be greater than the unity stoichiometric ratio, as opposed to those reported for ZnO films (0.63) [19] and nanosheets (0.86) [20]. The higher O percentage can therefore be attributed to the higher amount of hydroxide as also observed in the XPS analysis (shown later). The EDX spectrum also shows chlorine impurities in the sample arising from the supporting KCl electrolyte used in the electrodeposition, which have been proposed as an important capping component in controlling the anisotropic growth process [13].

Figure 2 shows the glancing-incidence XRD pattern of the as-grown ZnO nanowalls, along with a reference spectrum of ZnO powder (JCPDS 01-076-0704). All the major peaks obtained from ZnO nanowalls can be indexed to the wurtzite structure, with calculated lattice constants $a = b = 3.2497$ Å, $c = 5.2096$ Å, in excellent accord with the corresponding reference values ($a = b = 3.2530$ Å, $c = 5.2130$ Å). Unlike the case of 1D ZnO nanostructures which show preferential orientation in the (002) plane [7, 8], the relative peak intensities obtained for the ZnO nanowalls are well matched to those of the reference spectrum for powder ZnO, with (101) being the strongest peak. The peak width of the (101) plane is measured to be 0.406° FWHM, which indicates the highly crystalline nature of the nanowalls. The additional minor peaks seen in the XRD spectrum (figure 2) are also observed for leaf-

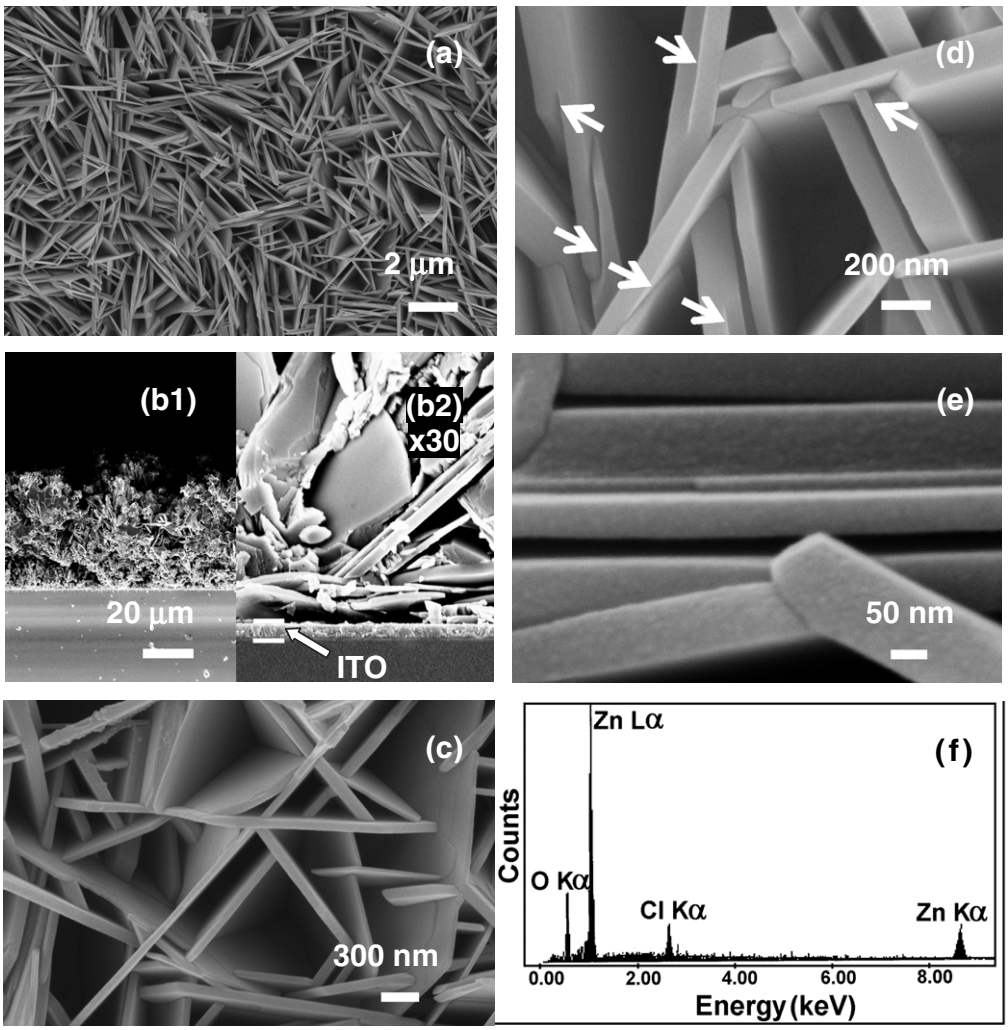

Figure 1. SEM images taken at different magnifications ((a), (c), (d), (e)) and EDX spectrum (f) of ZnO nanowalls electrodeposited for 1 h on an ITO–glass substrate at 70 °C. The arrows in (d) highlight the double-wall nanostructures. The corresponding cross-sectional images of the nanowalls are shown in (b1) and (b2) (in an exploded view), illustrating that the nanowalls grow directly on top of the ITO without any buffer layer of ZnO.

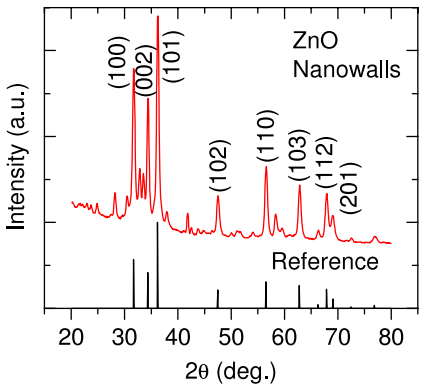

Figure 2. Glancing-incidence XRD spectrum of ZnO nanowalls electrodeposited on an ITO–glass substrate at 70 °C, along with the reference spectrum of ZnO powder (JCPDS 01-076-0704). The prominent crystallographic planes of the ZnO nanowalls are labeled.

(JCPDS 00-021-1486) and plate-like ZnO nanostructures [14]. It should be noted that these weak features do not match with any XRD features of chlorinated salts (arising from the supporting KCl electrolyte), which therefore rules out the presence of these chlorinated salts arising from the electrochemical deposition.

Figure 3 shows the O 1s XPS spectra of nanowalls as deposited and as a function of sputtering time. The O 1s envelope can be fitted to two components, corresponding to $Zn(OH)_2$ at a higher binding energy and ZnO at a lower binding energy [21, 22]. The binding energy difference of the two O 1s components is found to be 1.5 ± 0.1 eV, in good accord with that previously reported for a ZnO reference sample [23]. The presence of $Zn(OH)_2$ even after 300 s of sputtering is due to the nature of the reaction mechanism of the electrodeposition. This mechanism involves the hydroxylation reaction (i.e. formation of $Zn(OH)_2$) at the top surface of the as-grown nanostructures, followed by dehydration of $Zn(OH)_2$ to ZnO [24]. The higher Zn electrolyte concentration used in the present study favors faster hydroxylation reaction, leaving some $Zn(OH)_2$ unconverted in the dehydration reaction. The corresponding Zn 2p XPS spectra (not shown) show an intense Zn $2p_{3/2}$ ($2p_{1/2}$) feature, confirming the presence of a single

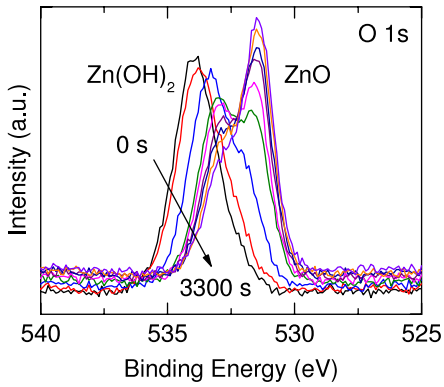

Figure 3. The O 1s XPS spectra of ZnO nanowalls deposited on ITO–glass at 70 °C and upon ion sputtering for 0, 30, 60, 180, 240, 300, 900, 1500 and 3300 s.

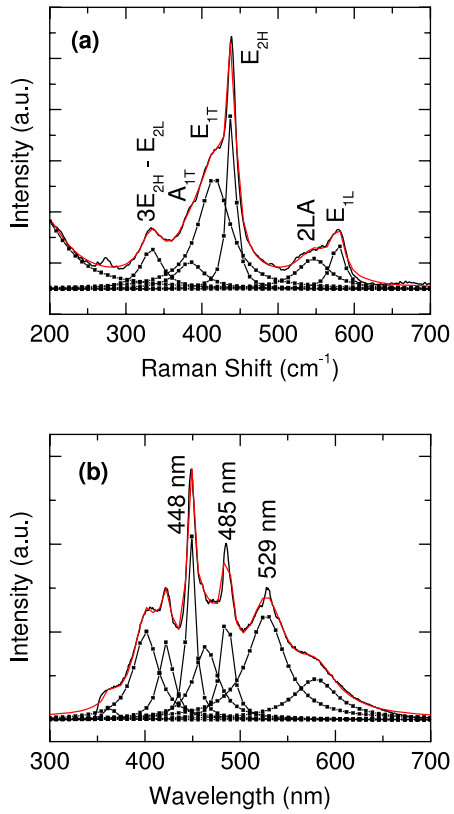

Figure 4. (a) Raman and (b) photoluminescence spectra of ZnO nanowalls electrodeposited on an ITO–glass substrate at 70 °C. The spectra have been fitted with the appropriate individual peaks in order to better identify the respective underlying spectral features.

Zn^{2+} divalent state that corresponds to both $Zn(OH)_2$ and ZnO. The observed spin–orbit splitting of 23.0 ± 0.1 eV is also evidently in good accord with the literature value of 22.97 eV [25].

The optical properties of the as-grown nanowalls are shown in figure 4. The Raman spectrum obtained with an excitation wavelength of 532 nm (figure 4(a)) has been fitted with the appropriate Lorentzian profiles (after appropriate background correction) and assigned in accord with the literature [9]. The spectral features for the nanowalls are found

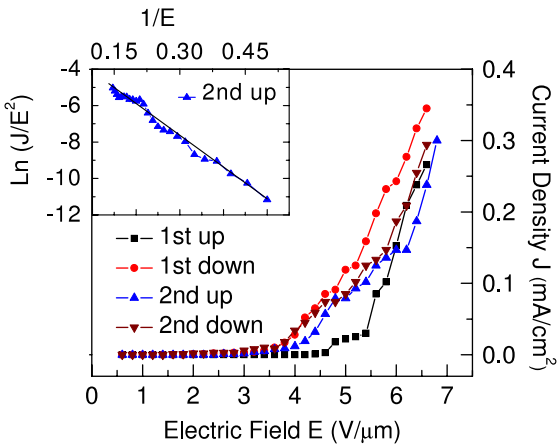

Figure 5. Field emission J–E characteristics of ZnO nanowalls electrodeposited on an ITO–glass substrate at 70 °C. The inset shows the Fowler–Nordheim plot of $\ln(J/E^2)$ versus $(1/E)$ for the second-up of applying field.

to be similar to those reported for ZnO nanowires [26] and nanosheets [9]. The most prominent feature at 438.5 cm^{-1} Raman shift corresponds to the E_{2H} mode of the wurtzite phase of ZnO structures [9, 26], consistent with our XRD result. The presence of the E_{1L} mode at 581 cm^{-1} Raman shift indicates an oxygen deficiency in the ZnO nanowalls, as also observed in the case of ZnO nanowires [27]. Figure 4(b) shows the corresponding photoluminescence spectrum collected at room temperature at an excitation wavelength of 254 nm. Unlike the 1D ZnO nanostructures that give a sharp UV band at ∼378 nm [7, 8, 28], the ZnO nanowalls exhibit multiple emission bands in the visible region, with the two strongest peaks at 448 and 485 nm. A relatively broad emission band at 529 nm is observed at a similar location to that reported for ZnO nanopencils [8]. For the curved nanowalls obtained by the thermal evaporation method [16], a broad photoluminescence feature, devoid of any sharp peaks, at 400–600 nm is observed. The sharp emissions in the visible region for the nearly vertical planar nanowalls observed in the present study are commonly attributed to the presence of various defects [20], in particular, the oxygen deficiency in ZnO as observed in the Raman spectrum.

Figure 5 shows the FE current density J as a function of the applied field E obtained for the ZnO nanowalls in four steps: the first ramping up of E (first-up), followed by ramping down (first-down), and similarly for the second cycle. The current density (0.34 mA cm^{-2}) for the ZnO nanowalls obtained at the maximum applied field of 6.6 V μm^{-1} used in the present work is found to be higher than those reported for ZnO nanoneedles (0.1 mA cm^{-2} at 24 V μm^{-1}) [28] and nanosheets (<0.1 mA cm^{-2} at 20 V μm^{-1}) [10]. From figure 5, we also determine the turn-on field, which is defined as the applied field at a current density of 0.1 μA cm^{-2}, in order to compare with the literature results. The turn-on field for the as-grown ZnO nanowalls is measured to be 4.8 V μm^{-1} in the first-up of applying field. As expected, the turn-on field comes down to 3.6 V μm^{-1} in the rest of the cycles, indicating that the surface becoming cleaner after the first-up step. The observed turn-on field for ZnO

nanowalls (3.6 V μm^{-1}) is therefore lower than that of ZnO needle-like nanowires (18 V μm^{-1}) [28], nanowires (8.0 V μm^{-1}) [29] and nanotubes (7.0 V μm^{-1}) [30], but higher than that of ZnO nanoneedles (2.4 V μm^{-1}) [31] and nanopins (1.92 V μm^{-1}) [32]. This is in accord with the general FE principle that the sharper the emitter tip is, the lower is the turn-on field. In the case of 1D nanostructures, the sharp emitter tips enhance the local field strength, allowing emission to occur at a lower applied field. The lower turn-on field from ZnO nanowalls can therefore be due to nanometer-thick upright walls, with emission likely to occur from the top edges of the nanowalls.

According to the Fowler–Nordheim relationship [30],

$$J = \frac{A\beta^2 E^2}{\phi} \exp\left(-\frac{B\phi^{3/2}}{\beta E}\right),$$

where the current density J is in units of A m^{-2}, the applied electric field E is in units of V m^{-1}, the work function ϕ of the emitter material is in units of eV, and the constants $A = 1.54 \times 10^{-6}$ A eV V^{-2} and $B = 6.83 \times 10^{9}$ $eV^{-3/2}$ V m^{-1}, we can obtain the field enhancement factor β by plotting $\ln(J/E^2)$ against $1/E$ (a so-called Fowler–Nordheim plot). The Fowler–Nordheim plot for the ZnO nanowalls shown as inset in figure 5 illustrates an almost linear behavior. Assuming ϕ is 5.3 eV for ZnO [30], the field enhancement factor is calculated to be 4700 from the slope of the straight line. The β value indicates the degree of FE enhancement of any tip over a flat surface, i.e. the true value of the electric field at the tip compared to its average macroscopic value. For a nanostructured emitter, the β value is related to the geometry, work function, conductivity and density of the nanostructures. In the present case of ZnO nanowalls, the calculated β value is found to be larger than most values reported for ZnO nanowires (300–2000) [4, 10, 28, 30, 33]. Even though the lateral dimension of the ZnO nanowalls is in the micrometer range, the nanometer-thin wall ledge (40-80 nm) and the substantial gap in between the walls (200–800 nm) might be contributing to it reaching the present high β value. It should be noted that the exceptionally high β value (41 000) reported by Jo *et al* [6] could be due to a combined effect of the high intrinsic aspect ratio of ZnO nanowires and the woven geometry of the carbon cloth substrate.

Emission stability is an important issue for applications in FE devices. Being an oxide material, ZnO is inherently more stable under practical operating conditions. Cheng *et al* have recently obtained a higher emission stability of ZnO nanoneedles than carbon nanotubes at a low air pressure [34]. Figure 6 shows the emission current density profile over a 90 min period at an applied field of 4.4 V μm^{-1} for the ZnO nanowalls (figure 1), which indicates a steady-state current density of 1.2 μA cm^{-2}. Evidently, there is a small increase and fluctuation in the emission current in the first 15 min of operation, which could be due to surface cleaning of the ZnO nanowalls. Interestingly, a slight increase in the current density is obtained after 70 min of continuous operation. The present stability test shows that the ZnO nanowalls do not have a tendency of gradual reduction in emission under a reasonable operating voltage, therefore suggesting that the ZnO nanowalls could be a promising material for FE applications.

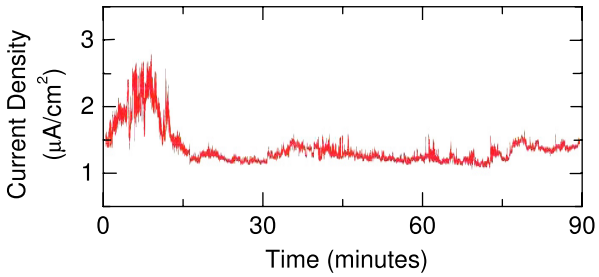

Figure 6. Stability profile of the current density of ZnO nanowalls over time under a constant applied field of 4.4 V μm^{-1} in a parallel-plate field emission set-up.

4. Summary

In conclusion, two-dimensional near-vertical planar ZnO nanowalls have been successfully fabricated on an ITO–glass substrate using a simple, cost-effective electrochemical deposition technique. XPS studies show that the nanowalls consist of ZnO covered with a $Zn(OH)_2$ overlayer. Glancing-incidence XRD reveals the highly crystalline wurtzite structure of the as-grown ZnO nanowalls. The well-defined wall-like structures with thickness 40–80 nm and length up to the micrometer scale are found to exhibit an excellent field emission property at a very low turn-on field of 3.6 V μm^{-1}. It is believed that electron emission takes place from the confined nanometer-thick ledge of the ZnO nanowalls. The formation of ZnO nanowalls at low temperature (70 °C) on an ITO–glass substrate and their high field emission performance make these novel two-dimensional nanostructures promising emitter materials for future display technology.

Acknowledgments

This work was financially supported by the Natural Sciences and Engineering Research Council of Canada, and the Japan Society for the Promotion of Science (Grants-in-aid for Scientific Research No. 18560661).

References

[1] Milne W I, Teo K B K, Amaratunga G A J, Legagneux P, Gangloff L, Schnell J-P, Semet V, Binh V T and Groening O 2004 *J. Mater. Chem.* **14** 933
[2] Fan S, Chapline M G, Franklin N R, Tombler T W, Cassell A M and Dai H 1999 *Science* **283** 512
[3] Pillai S C, Kelly J M, McCormack D E, O'Brien P and Ramesh R 2003 *J. Mater. Chem.* **13** 2586
[4] Ham H, Shen G Z, Cho J H, Lee T J, Seo S H and Lee C J 2005 *Chem. Phys. Lett.* **404** 69
[5] Dong L, Jiao J, Tuggle D W, Petty J M, Elliff S A and Coulter M 2003 *Appl. Phys. Lett.* **82** 1096
[6] Jo S H, Banerjee D and Ren Z F 2004 *Appl. Phys. Lett.* **85** 1407
[7] Li S Y, Lin P, Lee C Y and Tseng T Y 2004 *J. Appl. Phys.* **95** 3711
[8] Shen G, Bando Y, Liu B, Golberg D and Lee C J 2006 *Adv. Funct. Mater.* **16** 410
[9] Chen S, Liu Y, Shao C, Mu R, Lu Y, Zhang J, Shen D and Fan X 2005 *Adv. Mater.* **17** 586

[10] Cao B, Teng X, Heo S H, Li Y, Cho S O, Li G and Cai W 2007 *J. Phys. Chem.* C **111** 2470
[11] Cao B, Cai W, Zeng H and Duan G 2006 *J. Appl. Phys.* **99** 73516
[12] Illy B, Shollock B A, MacManus-Driscoll J L and Ryan M P 2005 *Nanotechnology* **16** 320
[13] Xu L, Guo Y, Lio Q, Zhang J and Xu D 2005 *J. Phys. Chem.* B **109** 13519
[14] Gao Y and Nagai M 2006 *Langmuir* **22** 3936
[15] Li F, Ding Y, Gao P X, Xin X and Wang Z L 2004 *Angew. Chem. Int. Edn* **116** 5350
[16] Lao J Y, Huang J Y, Wang D Z, Ren Z F, Steeves D, Kimball B and Porter W 2004 *Appl. Phys.* A **78** 539
[17] Kumar M, Kakamu K, Okazaki T and Ando Y 2004 *Chem. Phys. Lett.* **385** 161
[18] Jo S H, Tu Y, Huang Z P, Carnahan D L, Wang D Z and Ren Z F 2003 *Appl. Phys. Lett.* **82** 3520
[19] Tan S T, Sun X W, Zhang X H, Chua S J, Chen B J and Teo C C 2006 *J. Appl. Phys.* **100** 033502
[20] Hu J Q, Bando Y, Zhan J H, Li Y B and Sekiguchi T 2003 *Appl. Phys. Lett.* **83** 4414
[21] Bär M, Reichardt J, Sieber I, Grimm A, Kötschau I, Lauermann I, Sokoll S, Lux-Steiner M C, Fischer C H and Niesen T P 2006 *J. Appl. Phys.* **100** 23710
[22] Liu B and Zeng H C 2004 *J. Am. Chem. Soc.* **126** 16744
[23] Deroubaix G and Marcus P 1992 *Surf. Interface Anal.* **18** 39
[24] Izaki M and Omi T 1996 *J. Electrochem. Soc.* **143** L53
[25] Moulder J F, Stickle W F, Sobol P E and Bomben K D 1992 *Handbook of X-ray Photoelectron Spectroscopy* ed J Chastain (USA: Perkin-Elmer Corporation)
[26] Chen Y W, Liu Y C, Lu S X, Xu C S, Shao C L, Wang C W, Zhang J Y, Lu Y M, Shen D Z and Fan X W 2005 *J. Chem. Phys.* **123** 134701
[27] Wu J and Liu S C 2002 *J. Phys. Chem.* B **106** 9546
[28] Tseng Y K, Huang C J, Cheng H M, Lin I N, Liu K S and Chen I C 2003 *Adv. Funct. Mater.* **13** 811
[29] Yang Y H, Wang C X, Wang B, Xu N S and Yang G W 2005 *Chem. Phys. Lett.* **403** 248
[30] Wei A, Sun X W, Xu C X, Dong Z L, Yu M B and Huang W 2006 *Appl. Phys. Lett.* **88** 213102
[31] Zhu Y W, Zhang H Z, Sun X C, Feng S Q, Xu J, Zhao Q, Xiang B, Wang R M and Yu D P 2003 *Appl. Phys. Lett.* **83** 144
[32] Xu C X and Sun X W 2003 *Appl. Phys. Lett.* **83** 3806
[33] Xu F, Yu K, Shi M, Wang Q, Zhu Z and Huang S 2006 *J. Nanosci. Nanotechnol.* **6** 3794
[34] Cheng A J, Wang D, Seo H W, Liu C, Park M and Tzeng Y 2006 *Diamond Relat. Mater.* **15** 426